

## Analysis and Design of Compact Ultra-Wideband In-Phase/Out-of-Phase Power Dividers

Huy Ho-Sy-Nhat, Khac Kiem Nguyen, and Son Xuat Ta\*

**Abstract**—This paper presents the analysis and design of in-phase/out-of-phase power dividers with compact-size and ultra-wideband characteristics. The proposed designs are composed of a T-junction microstrip (MS)-to-slotline power divider with a shorting via and two slotline-to-MS transitions. The phase response at the outputs can be controlled by arranging the MS-line direction of the transition, i.e., the same direction results in the in-phase, whereas the opposite MS-line directions reverse the electrical field, thus resulting in the out-of-phase. Thanks to utilizing the MS-to-slotline power divider and circular slots and circular stubs at the transitions, the proposed structures achieve ultra-wide bandwidth and compact size simultaneously. The dividers are theoretically analyzed using transmission-line equivalent circuit, and then verified computationally and experimentally. Simulation and measurement indicate that the proposed power dividers yield ultra-wideband performance across 1.2–11.0 GHz ( $\sim 160\%$ ) with magnitude difference  $\pm 0.5$  dB and phase difference  $\pm 5^\circ$  at the outputs. As an example of application, a differential-fed Vivaldi antenna fed by the proposed out-of-phase power divider is implemented. The antenna yields a 160% bandwidth (1.2–11.0 GHz) for 10-dB return loss and a stable end-fire radiation within the whole impedance bandwidth.

### 1. INTRODUCTION

Power divider (PD), also known as a power splitter, is one of the fundamental microwave passive components involved in the wireless communication system [1]. Its function is to divide the initial signal into a number of signals with less power depending on the division ratio. For the output signals, there are two main aspects to be focused on: magnitude and phase responses. Due to the different types of phase responses at the outputs, the PDs can be classified as in-phase ( $0^\circ$ ), quadrature ( $90^\circ$ ), and out-of-phase ( $180^\circ$ ) types. As the magnitude and phase difference relationships can be modified within different configurations, such components are widely integrated in various parts of the wireless systems such as RF front ends, antenna feeding structures, power amplifiers, and mixers. To improve the data rate and capacity of wireless systems, all the involved components are required to yield a wide or even ultra-wide bandwidth [2], thus the PDs with ultra-wideband performance are indeed required to fulfill this demand.

To implement the wide-band PDs, the primary aim is to realize a wide-band transition between the input and outputs. The earliest literatures revolved Wilkinson power dividers by adding the combination of multi-stage and stepped impedance transmission lines [3–6]. These designs are capable of wide bandwidth, but their configurations are complex and require large layout areas. Another approach is to employ the strong coupling between different transmission-lines, such as microstrip (MS)-to-slot lines or slot-to-MS lines with closely placed locations [7–10]. The coupled-line designs can reduce the circuit's size while maintaining the wide-band characteristics. By inheriting the features of these

---

*Received 26 August 2022, Accepted 14 October 2022, Scheduled 25 October 2022*

\* Corresponding author: Son Xuat Ta (xuat.tason@hust.edu.vn).

The authors are with the School of Electrical and Electronic Engineering, Hanoi University of Science and Technology, Ha Noi 10000, Viet Nam.

transitions, several PDs [11–17] have been proposed for wideband wireless communication systems. Other techniques, such as substrate integrated waveguide loaded slots [18], parallel-coupled MS lines [19], and multilayer MS-to-slot transition [20], have been utilized to implement the wideband PDs. Most of the aforementioned PDs, however, yield only one type of phase response (i.e., either in-phase or out-of-phase) at the outputs. Also, the operational bandwidths of some previous PDs [11, 16, 18, 19], which are less than 60%, could be insufficient for the ultra-wide bandwidth applications [2].

In this paper, the analysis and design of compact PDs with in-phase/out-of-phase and ultra-wide bandwidth are presented. The proposed designs utilize MS-to-slotline transition technology, including T-junction MS-to-slotline PD and slot-to-MS transition, to achieve compact-size and wideband at the same time. The phase responses at the outputs are controlled by arranging the MS-line directions of the slot-to-MS transitions. The features of the proposed PDs are first analyzed by using transmission-line equivalent circuits and then verified via ANSYS Electronic Desktop and experiments. Finally, for illustrating an example of application, a differential-fed Vivaldi antenna fed by the proposed out-of-phase PD is implemented for an ultra-wide bandwidth and a stable end-fire radiation.

## 2. ANALYSIS AND DESIGN OF IN-PHASE/OUT-OF-PHASE POWER DIVIDERS

### 2.1. Geometry

The geometry of the proposed PDs is illustrated in Fig. 1. The designs are printed on both sides of RO4003 substrates ( $\epsilon_r = 3.38$ , thickness of 0.8128 mm, and  $\tan \delta = 0.0027$ ). The proposed PDs consist of a T-junction MS-to-slotline PD with a shorting-via and two slot-to-MS line transitions with circular slots and circular stubs. With these circular slot/stub realizations, the slot-to-MS line transition can obtain optimal bandwidth while maintaining the fabrication feasibility [10]. The MS lines and circular stubs are built on the topsides of the substrates, while the slotlines and circular slots are etched on the bottom-sides of the substrates. The input and outputs are MS-lines with characteristic impedance of 50-Ohm. The phase responses at the outputs are controlled by arranging the MS-line direction of the transition. As shown in Fig. 1, the output MS-lines of the in-phase PD have the same direction, whereas those of the out-of-phase PD have opposite directions. Both designs are optimized for a compact size and ultra-wide operational bandwidth. Their parameters are as follows:  $W_{ms1} = 1.75$ ,  $L_{s1} = 3$ ,  $L_{s2} = 5$ ,  $L_{s3} = 10$ ,  $L_1 = 15.4$ ,  $L_2 = 10.4$ ,  $s = 0.2$ ,  $D = 7.4$  (unit: mm).

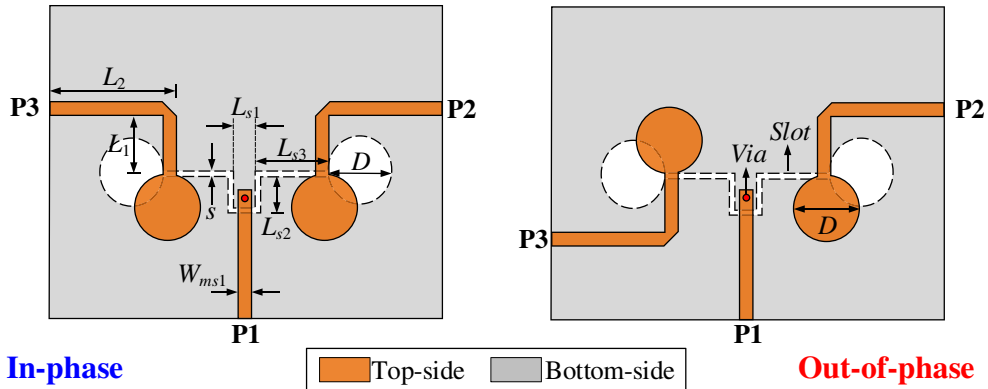
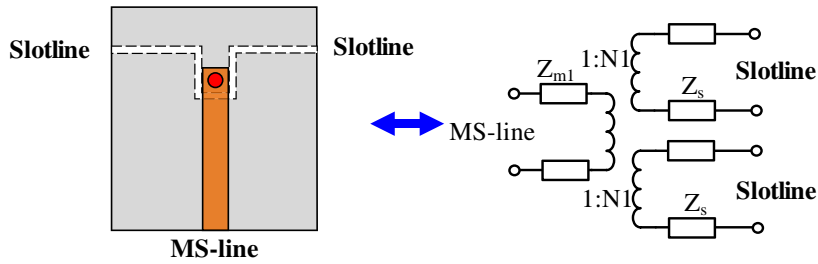


Figure 1. Geometry of the proposed power divider.

### 2.2. Analysis

Each proposed PD consists of a T-junction MS-to-slot line PD and two slot-to-MS transitions. For analyzing the operational mechanism, the PD and transitions are modeled using transmission line equivalent circuits as given in Figs. 2 and 3, respectively. As illustrated in Fig. 2, the T-junction PD can be considered as a three-port transformer [21], i.e., the input signal from the MS-line is equally



**Figure 2.** Transmission line equivalent circuit of the T-junction MS-to-slot line power divider.

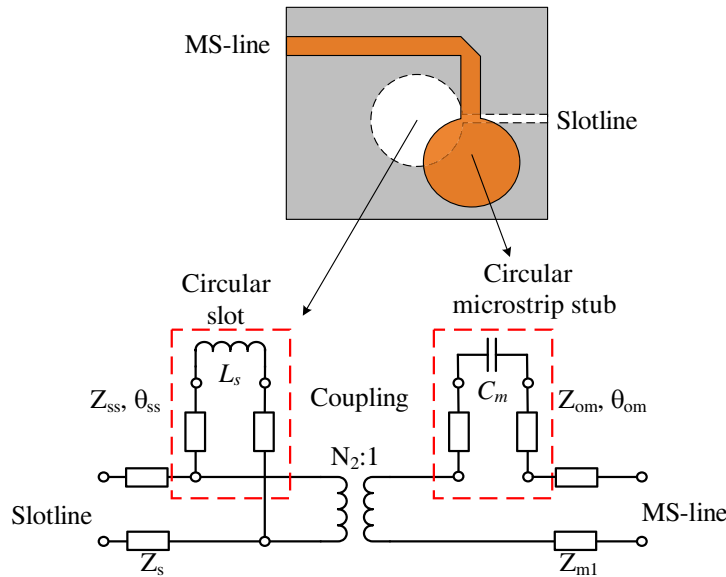


**Figure 3.** Transmission line equivalent circuit of the slot-to-MS line transition.

divided into balanced signals at the two slotlines through the MS-to-slot coupling, which is realized by using a shorted via. The input signal is divided into two output signals with a ratio of  $N_1$  expressed by:

$$N_1 = Z_s/Z_{m1} \tag{1}$$

where  $Z_s$  and  $Z_{m1}$  are the characteristic impedances of the slotline and MS-line, respectively. The equal power divider needs  $N_1 = 2$ , and consequently,  $Z_s = 2Z_{m1}$ . As shown in Fig. 3, the MS-to-slotline transition can be modeled using the magnetic coupling transition [10]. The circular slot is modeled using a series inductive load and stub with inductance  $L_s$  and electrical length  $\theta_{ss}$ . The circular MS stub is modeled using a series capacitive load and stub with capacitance  $C_m$  and electrical length  $\theta_{om}$ . With a suitable diameter of the circular slot and stub, i.e.,  $D$  of about  $4W_{ms}$ , the values of  $L_s$  and  $C_m$  can be neglected [15], while the values of  $\theta_{ss}$  and  $\theta_{om}$  can be chosen about a quarter-wavelength at the center frequency of 6.0 GHz. At the transitions, the signal transits from the slotline to the MS line with the transformer ratio of  $N_2$  [15], which is expressed by:

$$N_2^2 = Z_{m2}/Z_s \tag{2}$$

where  $Z_{m2}$  and  $Z_s$  are the characteristic impedances of the output MS line and the slotline, respectively.

Using the equivalent circuits in Figs. 2 and 3, the proposed in-phase/out-of-phase PDs can be modeled by transmission-line equivalent circuits, as shown in Fig. 4. The two schematics are characterized by using Keysight Advanced Design System (ADS). To model the out-of-phase response, the electrical fields at the output MS-lines are assigned with different directions, as shown in Fig. 4(b). For all calculated frequencies, the input/output MS-lines have the characteristic impedance of  $Z_{m1} =$

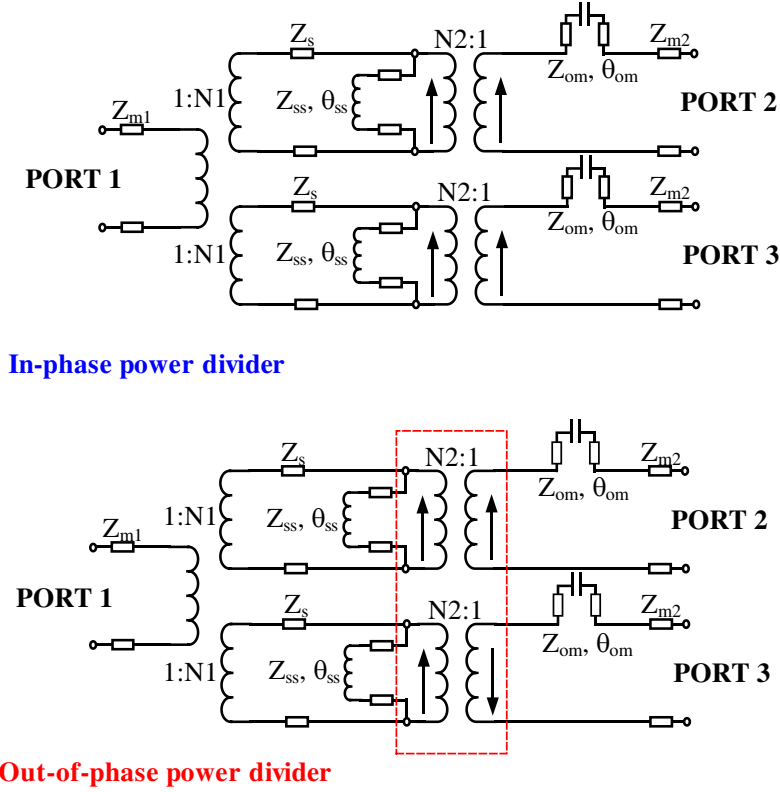


**Figure 4.** Transmission line equivalent circuit of the in-phase/out-of-phase power dividers.

$Z_{m2} = 50\text{-}\Omega$ . Since the ADS software does not provide the slotline model, the slotlines are modeled as the MS-lines in the equivalent circuits. To mitigate the fabrication errors, the slotlines with  $s = 0.2\text{ mm}$  are fixed. On the other hand, the characteristic impedance of the slotline is dependent on the frequency [22]. Accordingly, in the ADS calculations, the  $Z_s$ ,  $N_1$ , and  $N_2$  values are adapted for each frequency, as listed in Table 1. The ADS calculated results of the two equivalent circuits are given in Fig. 5. The ADS calculations indicate that the two PDs theoretically achieve perfect performances, i.e., at all calculated frequencies, the reflection coefficients at the input ports ( $|S_{11}| < -12\text{ dB}$ ), equally divided powers ( $|S_{21}| = |S_{31}|$ ), the phase differences ( $\text{ang } S_{21} - \text{ang } S_{31}$ ) of  $0^\circ$  and  $180^\circ$  for the in-phase and out-of-phase designs, respectively.

**Table 1.** Slotline impedances ( $Z_s$ ), divided ratio ( $N_1$ ), and transformer ratio ( $N_2$ ) of the equivalent circuits for different frequencies in the ADS calculations.

Freq. (GHz)	1	2	3	4	5	6	7	8	9	10	11
$Z_s$ ( $\Omega$ )	77.0	84.8	85.5	88.6	91.3	93.7	95.9	97.9	99.8	101.7	103.4
$N_1$	1.54	1.63	1.71	1.76	1.82	1.87	1.91	1.96	1.99	2.02	2.06
$N_2$	0.80	0.78	0.76	0.75	0.74	0.73	0.72	0.71	0.7	0.68	0.69

### 2.3. Simulation and Measurement Results

To verify the theoretical results obtained by using the equivalent circuits, the proposed in-phase/out-of-phase PDs are characterized using the full-wave simulator of ANSYS Electronics Desktop, and then fabricated and tested. Their simulated and measured results are given in Figs. 6 and 7. The prototypes [Figs. 6(a) and 7(a)] are realized on the  $40\text{ mm} \times 50\text{ mm}$  RO4003 pieces with a copper sheet of 0.5-Oz

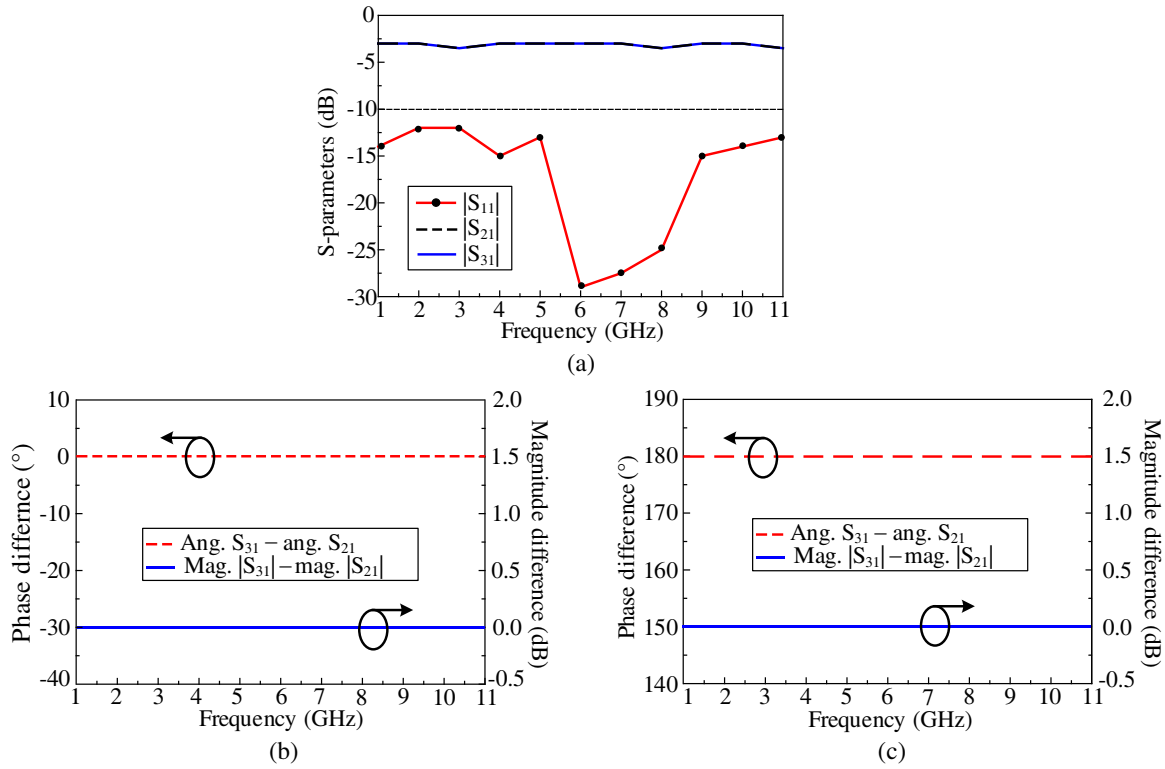


**Figure 5.** ADS calculated results of the transmission-line equivalent circuits: (a)  $S$ -parameters; phase and magnitude differences at outputs of (b) in-phase and (c) out-of-phase power divider.

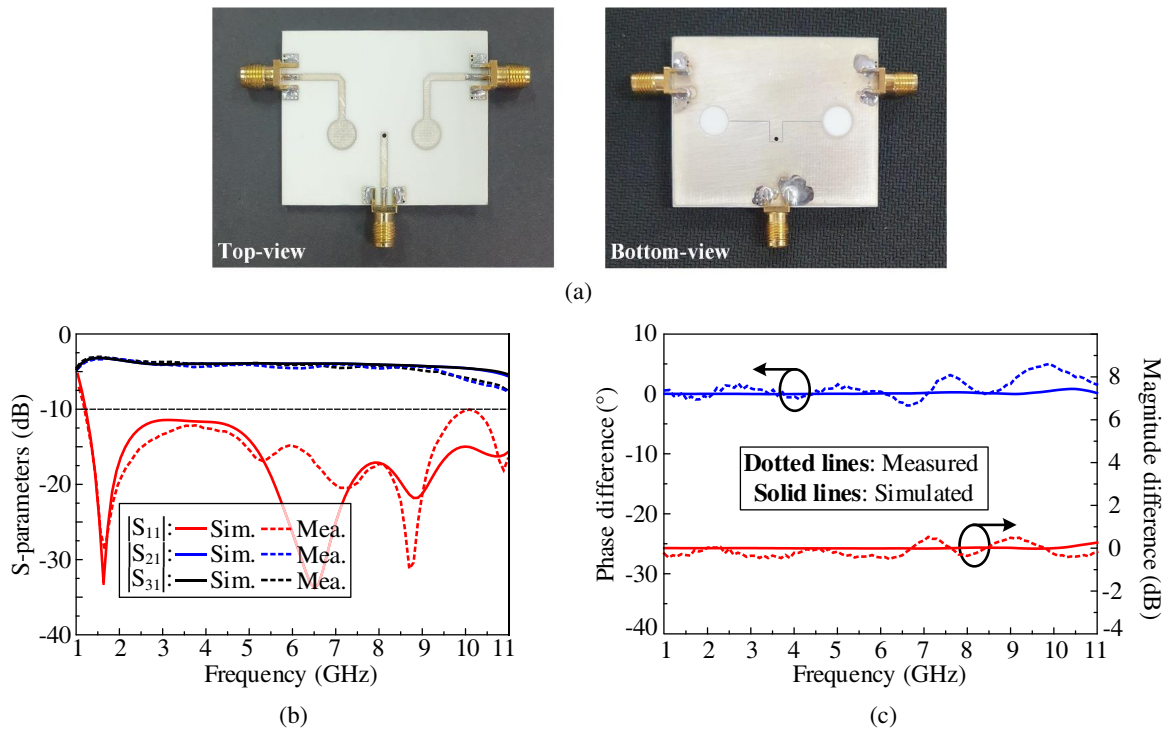


**Figure 6.** (a) Fabricated prototype of in-phase power dividers and its simulated and measured results: (b)  $S$ -parameters and (c) phase and magnitude differences at the outputs.

thickness using printed circuit board (PCB) technology. Sub-Miniature version A (SMA) connectors are used as the coaxial-to-MS transformers.

The performances of the in-phase PD are shown in Figs. 6(b) and 6(c). Both simulation and measurement indicate that the prototype yields  $|S_{11}| < -10$  dB at 1.2–11.0 GHz (160%), nearly equally divided powers, and in-phase at the outputs. Nevertheless, the measured magnitude and phase differences are  $\pm 0.5$  dB and  $\pm 5^\circ$ , respectively. As shown in Fig. 7(b), the out-of-phase PD yields  $|S_{11}| < -10$  dB and  $|S_{21}| = |S_{31}|$  from 1.2–11.0 GHz (160%). As shown in Fig. 7(c), the measurements result in magnitude and phase differences at the outputs of  $\pm 0.5$  dB and  $180 \pm 3.5^\circ$ , respectively. From Figs. 6(c) and 7(c), the measured magnitude and phase differences at the outputs are greater than the simulated values, which could be attributed to the effects of SMA connectors and fabrication imperfection.

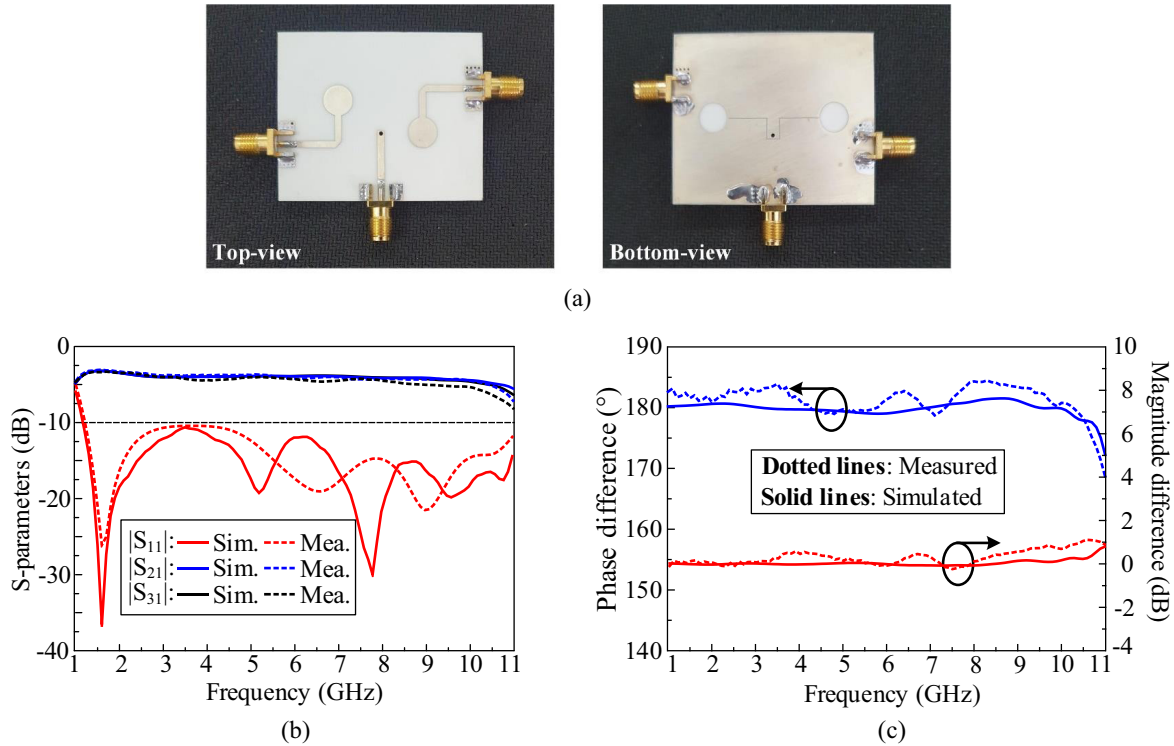


**Figure 7.** (a) Fabricated prototype of out-of-phase power dividers and its simulated and measured results: (b)  $S$ -parameters and (c) phase and magnitude differences at the outputs.

#### 2.4. Comparison

A comparison between the proposed power dividers and the related priors is given in Table 2. For a fair comparison, all designs are implemented on the single-layer substrates and can be easily fabricated using the PCB technology. It is observed that the proposed designs yield a more compact size, wider operational bandwidth, and comparable differences at the outputs relative to the previous works.

### 3. ULTRA-WIDEBAND VIVALDI ANTENNA USING OUT-OF-PHASE POWER DIVIDER

For illustrating an application example of the proposed PDs, in this section, a differential-fed Vivaldi antenna using the out-of-phase PD is designed, realized, and tested. The Vivaldi antenna is selected due to its simple configuration, ultra-wide bandwidth, and stable end-fire radiation [23–27]. Some Vivaldi antennas, e.g., [23–25], are composed of radiating flares printed on different-sides of the substrate, which

**Table 2.** Comparison between the proposed PDs and the priors.

Designs	Dimension ( $\lambda_{min}^2$ )	Bandwidth (%)	Magnitude difference (dB)	Phase difference ( $^\circ$ )
Proposed In-phase design	$0.2 \times 0.16$	160.0	$\pm 0.5$	$\pm 5^\circ$
Proposed out-of-phase design	$0.2 \times 0.16$	160.0	$\pm 0.5$	$180^\circ \pm 3.5^\circ$
[11]	$0.26 \times 0.20$	57.1	$\pm 0.5$	$\pm 5^\circ$
[12]	$0.31 \times 0.25$	109.5	$\pm 0.5$	$180^\circ \pm 2.5^\circ$
[13]	$0.24 \times 0.19$	109.7	$\pm 0.5$	$180^\circ \pm 2.4^\circ$
[14]	$0.22 \times 0.28$	100.0	$\pm 1.0$	$80^\circ \pm 2^\circ$
[15]	$0.30 \times 0.41$	136.8	$\pm 0.5$	$180^\circ \pm 5^\circ$
[16]	$1.10 \times 0.66$	48.1	Not mentioned	$180^\circ \pm 5^\circ$
[17]	Not mentioned	141.5	$\pm 1.05$	$180^\circ \pm 5^\circ$
[18]	$1.45 \times 1.45$	56.0	$\pm 0.8$	Not mentioned
[19]	$0.25 \times 0.25$	57.0	$\pm 0.5$	$\pm 2.5^\circ$

$\lambda_{min}$  is the free-space wavelength referring to the lowest operational frequency.

could cause a high cross-polarization level. This problem can be solved by using a differential-fed Vivaldi antenna with radiating flares symmetrically printed on the same plane [26, 27]. This differential-feed is realized by using two balanced signals with the same magnitude and  $180^\circ$  phase difference, which are mainly challenging to fulfill ultra-wide frequency range. Accordingly, the proposed out-of-phase PD is a good candidate to overcome this challenge.

### 3.1. Antenna Geometry

Figure 8 illustrates the geometry of Vivaldi antenna fed by an out-of-phase PD. It consists of two radiating flares symmetrically printed on the top side of the RO4003 substrate ( $\epsilon_r = 3.38$ , thickness of 0.8128 mm, and  $\tan \delta = 0.0027$ ). The two flares are connected to the output MS lines of the proposed out-of-phase PD. At the starting points, the flares have strip-width of 0.2-mm and gap of 0.2-mm. Each flare is shaped regarding the inner and outer curves, as shown in Fig. 8. The inner curves can be divided into two main parts, i.e., Section 1 and Section 2. The exponential curve of Section 1 is defined by the following parametric equation in the  $y$ - $z$  plane:

$$\frac{\lambda_{center}}{2} < W_{in} < \frac{\lambda_{min}}{2} \tag{3}$$

$$y = \pm (C_1 e^{-z} + C_2) \tag{4}$$

$$C_1 = \frac{y_2 - y_1}{e^{z_2} - e^{z_1}} \tag{5}$$

$$C_2 = \frac{y_1 e^{Az_2} - y_2 e^{z_1}}{e^{Az_2} - e^{Az_1}} \tag{6}$$

where the opening width ( $W_{in}$ ) is chosen in the range in (3) according to the design guideline for the Vivaldi antenna in [23]. The curve positions are limited by the starting points ( $z_1, \pm y_1$ ) and ending

points  $(z_2, \pm y_2)$ , regarding the origin  $(0, 0)$ . The position points are given by:

$$(z_2, y_2) = \begin{cases} y_2 = \frac{(W - W_{in})}{2} \\ z_2 = 0 \end{cases} \quad (7)$$

$$(z_1, y_1) = \begin{cases} y_1 = \frac{(W - W_m)}{2} \\ z_1 = L_{in} + L_{out} - L_m \end{cases} \quad (8)$$

On the other hand, Section 2 can be realized as a reversed isosceles triangle with the base's length ( $W_m$ ) and height ( $L_m$ ). The outer curve (Section 3) is formed in a quarter of an ellipse with minor ( $L_{out}$ ) and major ( $W_{out}$ ) radii, here,  $W_{out} = 1.85L_{out}$ . The antenna is characterized via the ANSYS Electronics Desktop for an ultra-wideband operation and a stable end-fire radiation. To adapt the radiating flares, the out-of-phase PD is slightly modified as compared to the prototype given in Fig. 7. Referring to Figs. 1 and 8, the final design parameters of the Vivaldi antenna are as follows:  $W_{in} = 58$ ,  $L_{in} = 89$ ,  $W_{out} = 59.2$ ,  $L_{out} = 32$ ,  $W_m = 11.2$ ,  $L_g = 29$ ,  $W_{ms} = 1.75$ ,  $L_{s1} = 3$ ,  $L_{s2} = 5$ ,  $L_{s3} = 10$ ,  $L_1 = 15.4$ ,  $L_2 = 10.4$ ,  $s = 0.2$ ,  $D = 7.4$  (unit: mm).

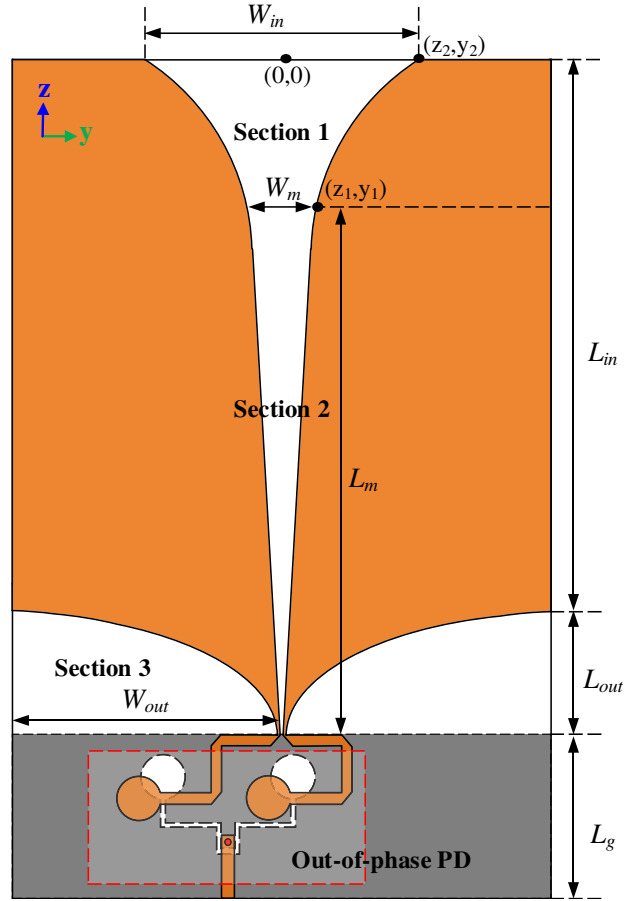


**Figure 8.** Geometry of differential-fed Vivaldi antenna fed by out-of-phase power divider.

### 3.2. Simulation and Measurement Results

The Vivaldi antenna fed by out-of-phase PD has been fabricated and measured. Fig. 9(a) shows the fabricated antenna prototype with measuring dimension of  $150 \text{ mm} \times 98 \text{ mm}$  ( $0.58\lambda_{\min} \times 0.38\lambda_{\min}$ , where  $\lambda_{\min}$  is the wavelength at the lowest operational frequency). Fig. 9(b) depicts the measured and

simulated  $|S_{11}|$  values of the antenna prototype. There is a good agreement between the simulation and measurement, and both indicate that the antenna prototype achieves an ultra-wide bandwidth, i.e., the simulated and measured  $|S_{11}|$  values are less than  $-10$  dB at 1.2–11.0 GHz (160%). There is a minor breach where the measured  $|S_{11}|$  is slightly greater than  $-10$  dB around 1.8 GHz, which could be attributed to the fabrication tolerances.

Figure 9(b) also illustrates the simulated realized gain of the antenna prototype. It is observed that the antenna yields a small gain variation within a wide frequency range. Its 3-dB gain bandwidth is 123% (2.5–10.5 GHz), and the peak gain is 10.5 dBi. Moreover, the simulations indicate that the antenna achieves a table end-fire radiation within the impedance matching bandwidth. For brevity, Fig. 10 only shows the normalized radiation patterns at 2, 6, and 10 GHz. At all the frequencies, the antenna yields a highly symmetrical pattern, high front-to-back ratio, and low cross-polarization level at the end-fire direction.

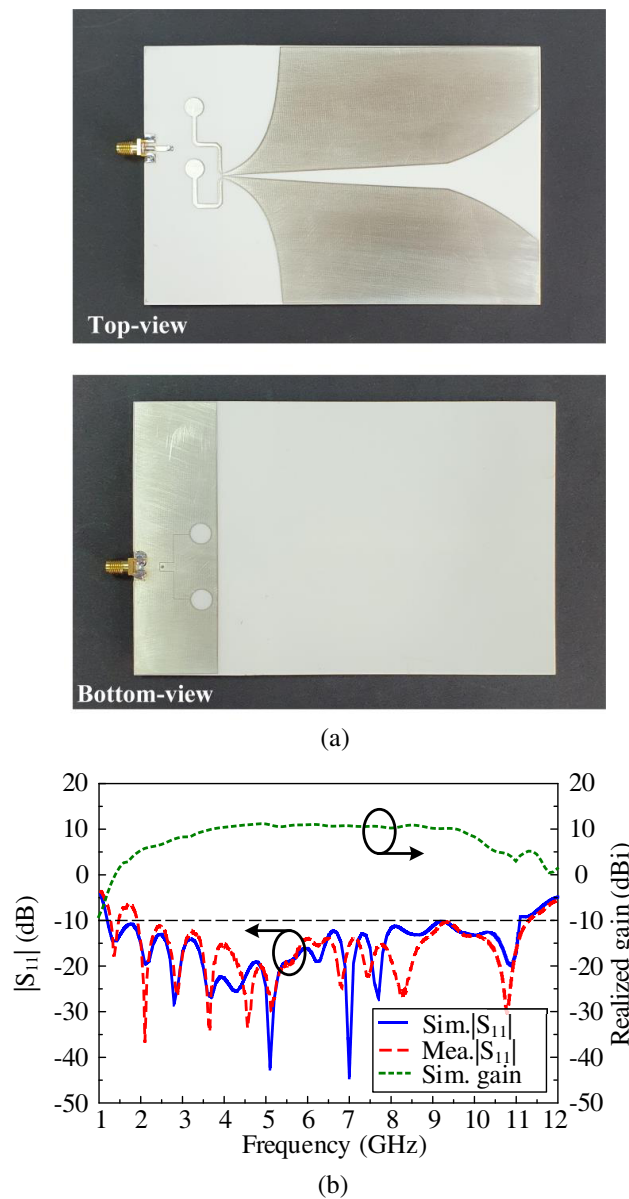


**Figure 9.** (a) Fabricated prototype of the Vivaldi antenna and (b) its  $|S_{11}|$  and realized gain.

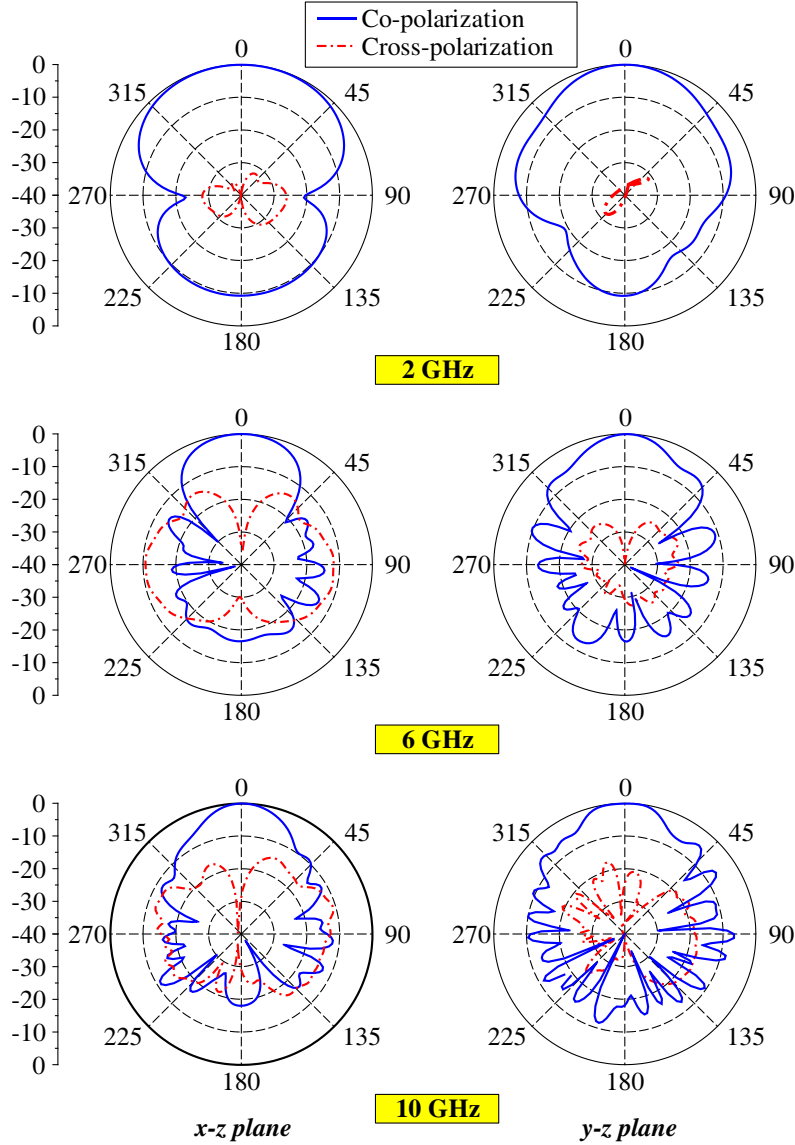


**Figure 10.** Simulated normalized radiation pattern of the Vivaldi antenna.

#### 4. CONCLUSION

The paper has described the analysis and design of compact in-phase and out-of-phase PDs with ultra-wideband characteristic. Their basic configuration consists of an MS-to-slotline PD with a shorting-via and two slotline-to-MS transitions with circular slots and stubs, which allow the ultra-wide bandwidth and compact size at the same time. Their features are first analyzed by using a transmission-line equivalent circuit and then validated computationally and experimentally. The final PD prototypes with size of  $0.2\lambda_{\min} \times 0.16\lambda_{\min}$  achieve an operational bandwidth of 1.2–11.0 GHz (160%) with the magnitude difference of  $\pm 0.5$  dB and phase difference of  $\pm 5^\circ$  at the outputs. With the advantages of compact size, simple configuration, wideband, and in-phase/out-of-phase, the proposed PDs can be widely used in ultra-wideband applications. For an example of application, a differential-fed Vivaldi antenna using the proposed out-of-phase power divider is designed, fabricated, and measured. The antenna prototype achieves an impedance bandwidth of 160% (1.2–11.0 GHz) and a stable end-fire radiation with 3-dB gain bandwidth of 123% (2.5–10.5 GHz) and the peak gain of 10.5 dBi.

## REFERENCES

1. Wu, Y., L. Jiao, Z. Zhuang, and Y. Liu, "The art of power dividing: A review for state-of-the-art planar power dividers," *China Communications*, Vol. 14, No. 5, 1–16, May 2017.
2. Federal Communications Commission, "Revision of part 15 of the commission's rules regarding UWB transmission systems," *First Report*, FCC 02-48, 2002.
3. Wilkinson, E. J., "An N-way hybrid power divider," *IRE Transactions on Microwave Theory and Techniques*, Vol. 8, No. 1, 116–118, Jan. 1960.
4. Ju, I., M. Cho, I. Song, and J. D. Cressler, "A compact, wideband lumped-element Wilkinson power divider/combiner using symmetric inductors with embedded capacitors," *IEEE Microwave and Wireless Components Letters*, Vol. 26, No. 8, 595–597, Aug. 2016.
5. Oraizi, H. and A. R. Sharifi, "Design and optimization of broadband asymmetrical multisection Wilkinson power divider," *IEEE Transactions on Microwave Theory and Techniques*, Vol. 54, No. 5, 2220–2231, May 2006.
6. Honari, M. M., L. Mirzavand, R. Mirzavand, A. Abdipour, and P. Mousavi, "Theoretical design of broadband multisection wilkinson power dividers with arbitrary power split ratio," *IEEE Transactions on Components, Packaging and Manufacturing Technology*, Vol. 6, No. 4, 605–612, Apr. 2016.
7. Ahmed, U. T. and A. M. Abbosh, "Wideband out-of-phase power divider using tightly coupled lines and microstrip to slotline transitions," *Electronics Letters*, Vol. 52, No. 2, 126–128, 2016.
8. Henin, B. and A. Abbosh, "Wideband hybrid using three-line coupled structure and microstrip-slot transitions," *IEEE Microwave and Wireless Components Letters*, Vol. 23, No. 7, 335–337, Jul. 2013.
9. Shen, X., Y. Liu, S. Zhou, and Y. Wu, "A novel compact tunable coupled-line power divider using varactors," *2015 Asia-Pacific Microwave Conference (APMC)*, 1–3, 2015.
10. Shuppert, B., "Microstrip/slotline transitions: Modeling and experimental investigation," *IEEE Transactions on Microwave Theory and Techniques*, Vol. 36, No. 8, 1272–1282, Aug. 1988.
11. Ahmed, U. T. and A. M. Abbosh, "Compact single-layer in-phase power divider employing microstrip to slotline transitions," *2014 1st Australian Microwave Symposium (AMS)*, 13–14, 2014.
12. Bialkowski, M. E. and A. M. Abbosh, "Design of a compact UWB out-of-phase power divider," *IEEE Microwave and Wireless Components Letters*, Vol. 17, No. 4, 289–291, Apr. 2007.
13. Zhu, H., Z. Cheng, and Y. J. Guo, "Design of wideband in-phase and out-of-phase power dividers using microstrip-to-slotline transitions and slotline resonators," *IEEE Transactions on Microwave Theory and Techniques*, Vol. 67, No. 4, 1412–1424, Apr. 2019.
14. Xiao, B., H. Yao, M. Li, J. -S. Hong, and K. L. Yeung, "Flexible wideband microstrip-slotline-microstrip power divider and its application to antenna array," *IEEE Access*, Vol. 7, 143973–143979, 2019.
15. Horestani, A. K. and Z. Shaterian, "Ultra-wideband balun and power divider using coplanar waveguide to microstrip transitions," *International Journal of Electronics and Communications*, Vol. 95, 297–303, 2018.
16. Xu, H.-T., et al., "A wideband out-of-phase power divider based on odd-mode spoof surface plasmon polaritons," *2020 International Conference on Microwave and Millimeter Wave Technology (ICMMT)*, 1–3, 2020.
17. Ghimire, J. and D.-Y Choi, "Ultra-wide band double-slot podal and anti-podal Vivaldi antennas feed by compact out-of-phase power divider slot for fluid properties determination," *Sensors*, 4543, 2022.
18. Kumari, G. and R. K. Barik, "Compact out-of-phase wideband substrate integrated waveguide based power divider loaded by slots for Ku and K band applications," *2019 International Conference on Communication and Signal Processing (ICCSP)*, 0396–0399, 2019.
19. Ahmed, U. T. and A. M. Abbosh, "Compact single-layer in-phase power divider employing microstrip to slotline transitions," *2014 1st Australian Microwave Symposium (AMS)*, 13–14, 2014.

20. Xiao, L., H. Peng, and T. Yang, "Compact ultra-wideband in-phase multilayer power divider," *Progress In Electromagnetics Research Letters*, Vol. 48, 33–37, 2014.
21. Miller, G., "TF3 (3-Port Transformer)," Sep. 10, 2008, [Online]. Available [Last accessed: Aug. 26, 2022]: <https://edadocs.software.keysight.com/pages/viewpage.action?pageId=5924503>.
22. Janaswamy, R. and D. H. Schaubert, "Characteristic impedance of a wide slotline on low-permittivity substrates (short paper)," *IEEE Transactions on Microwave Theory and Techniques*, Vol. 34, No. 8, 900–902, Aug. 1986.
23. Azim, R., M. T. Islam, and N. Misran, "Compact tapered-shape slot antenna for UWB applications," *IEEE Antennas and Wireless Propagation Letters*, Vol. 10, 1190–1193, 2011.
24. Amiri, M., F. Tofigh, A. Ghafoorzadeh-Yazdi, and M. Abolhasan, "Exponential antipodal Vivaldi antenna with exponential dielectric lens," *IEEE Antennas and Wireless Propagation Letters*, Vol. 16, 1792–1795, 2017.
25. Dai, L. H., T. Zhou, Z. R. Liang, and Y. Jin Zhou, "Miniaturized broadband antipodal Vivaldi antenna with high gain and its array," *2019 International Symposium on Antennas and Propagation (ISAP)*, 1–3, 2019.
26. Guo, J., T. Djerafi, and K. Wu, "Balanced corrugated antipodal linear tapered slot antenna with integrated feeding for cross-polarization suppression," *18th International Symposium on Antenna Technology and Applied Electromagnetics (ANTEM)*, 1–4, 2018.
27. Eichenberger, J., E. Yetisir, and N. Ghalichechian, "High-gain antipodal Vivaldi antenna with pseudo element and notched tapered slot operating at (2.5 to 57) GHz," *IEEE Transactions on Antennas and Propagation*, Vol. 67, No. 7, 4357–4366, Jul. 2019.